Applied Catalysis B: Environmental 174–175 (2015) 533–543

Contents lists available at ScienceDirect

Applied Catalysis B: Environmental

journal homepage: www.elsevier.com/locate/apcatb

Enhanced photoactive and photoelectrochemical properties of TiO_2 sol–gel coated steel by the application of SiO_2 intermediate layer

Juha-Pekka Nikkanen[a,*], Elina Huttunen-Saarivirta[a,1], Turkka Salminen[b], Leo Hyvärinen[a], Mari Honkanen[a], Elisa Isotahdon[a], Saara Heinonen[a], Erkki Levänen[a]

[a] Department of Materials Science, Tampere University of Technology, P.O. Box 589, FIN-33101 Tampere, Finland
[b] Optoelectronics Research Centre, Tampere University of Technology, P.O. Box 692, 33101 Tampere, Finland

ARTICLE INFO

Article history:
Received 20 November 2014
Received in revised form 3 March 2015
Accepted 10 March 2015
Available online 13 March 2015

Keywords:
Titanium dioxide
Photocatalysis
Substrate
Electrical resistance
Electrochemical impedance spectroscopy

ABSTRACT

Photocatalysis is a promising solution for purifying air and water from pollutants, yet more efficient photocatalytic materials are needed. A new approach is proposed in this paper for enhancing the photoactive and photoelectrical properties of anatase TiO_2 films by applying an intermediate SiO_2 film between the TiO_2 film and the stainless steel substrate. TiO_2 and SiO_2 coatings are synthesized by a sol–gel method and the thickness of TiO_2 film is varied in order to obtain improved understanding on the role of thickness in photocatalytic and electrochemical performance. The obtained coatings are systematically characterized in terms of microstructure using such techniques as field-emission scanning electron microscopy (FE-SEM), Raman spectroscopy and X-ray diffraction (XRD), that demonstrate, e.g., the anatase phase structure of the TiO_2 films. The enhanced photocatalytic properties of SiO_2/TiO_2 coatings as compared to TiO_2 films are verified using methylene blue (MB) discoloration tests, while the improved photoelectrochemical properties are shown by potentiodynamic i–V scans, open circuit potential (OCP) monitoring and electrochemical impedance spectroscopy (EIS). We attribute the beneficial effect of the intermediate SiO_2 film on the photocatalytic and photoelectrochemical performance to the high electrical resistance of the SiO_2 that imposes a high-energy barrier for electron transfer and, therefore, (partly) insulates the TiO_2 film from the substrate and acts as a capacitor for photo-generated electrons under illumination. The presented results show an effective way of enhancing the photocatalytic performance of anatase TiO_2 films.

1. Introduction

Environmental pollution has become a tremendous problem during the past years. Air and water pollutants produced by human activity cause serious harm to living organisms all over the world [1–3]. For example, waste waters released into the environment by textile industry are known to contain high amounts of dyes which may cause adverse effects on the ecosystem due to their toxicity [4,5]. Among other methods, photocatalysis has been proposed to be an effective way to purify air and water from organic and inorganic detrimental elements and compounds [1–6].

Titanium dioxide (TiO_2) is a photocatalytic material that has been widely studied due to its redox properties, chemical stability, and non-toxicity [7]. TiO_2 is applied in the purification of water and air, [8,9] solar power systems, [10,11] lithium batteries, [12] and self-cleaning and antifogging surfaces [13,14]. The key photocatalytically active polymorphs of TiO_2 are anatase and rutile [15]. The anatase phase is usually considered a more photoactive polymorph although the rutile phase is used in some applications due to its better photo-absorption properties in the visible light wavelength range [16,17]. However, the mobility of charge carriers in the rutile structure is hindered by regiment of recombination centers which makes rutile a quite inactive photocatalyst [18,19].

TiO_2 is normally used in photocatalytic applications as powder mixed in the system or coating deposited on a solid substrate. Various wet-chemistry methods for the production of TiO_2 powders include sol–gel based, i.e., hydrothermal, solvothermal, and low-temperature synthesis, routes [16,20–25]. Another common approach to produce TiO_2 and various other metal oxide powders is a liquid flame spray technique [26–28]. However, the use of TiO_2 powder may be complicated. For example, when TiO_2 powder is used in the purification of water, the powder has to be removed

* Corresponding author. Tel.: +358 407195634.
E-mail address: juha-pekka.nikkanen@tut.fi (J.-P. Nikkanen).
[1] At present: VTT Technical Research Centre of Finland, Materials Performance, P.O. Box 1300, FI-33101 Tampere, Finland.

http://dx.doi.org/10.1016/j.apcatb.2015.03.014
0926-3373/

from the water after the purification process. It is easy to understand that the removal of nanosized powder from a solution is very demanding [29]. Application of TiO_2 photocatalyst as a thin film on a solid surface helps to overcome this disadvantage [30]. Indeed, the production of TiO_2 based photocatalytic coatings has attracted a great deal of attention during the past years [30–34]. The lessons learned are that the photocatalytic activity of the TiO_2 coatings depends on many variables, including the characteristics of the substrate [30–32]. First, it has been found that the diffusion of sodium and calcium ions from soda-lime glass substrate into the TiO_2 films prepared at 500 °C is detrimental to the photocatalytic activity of the films. However, the diffusion of sodium and calcium ions can be effectively inhibited by the interfacial layer of SiO_2 [30]. It has also been concluded that the diffusion of sodium ions from the soda-lime glass to the TiO_2 coating has a detrimental effect on the anatase nanostructure [31]. Second, the comparison of the photocatalytic activity of TiO_2 coatings produced on glass, quartz, and stainless steel substrates has been shown to decrease in the following order: TiO_2/quartz > TiO_2/stainless steel ~TiO_2/glass [32]. However, the coatings used on the three substrates differed in terms of phase structure: pure anatase phase covered the glass and quartz substrates, but a mixture of anatase and rutile phases was detected on stainless steel, making it ambiguous to conclude that the detected photocatalytic activities depend on the substrates only [32]. Third, some recent results, e.g., [35] indicate that the interfacial electrically resistive layer between the conductive substrate and the photoactive TiO_2 layer would be beneficial for the photocatalytic properties of the system, but no systematic research has been performed on the topic. In this study, we try to fill this gap. For this, TiO_2 coatings were prepared by a sol–gel method on stainless steel substrate with and without an intermediate electrically resistive layer of SiO_2. The prepared samples were then systematically characterized in terms of microstructure, photocatalytic activity, and photoelectrochemical properties. In this paper, the results from such characterization are presented and discussed.

2. Experimental

2.1. Preparation of samples

Plates of austenitic stainless steel EN 1.4301/AISI 304 (25 mm × 75 mm × 0.75 mm) were used as the substrate material in this work. The plates exhibited a standard surface finish 2B, being hence cold rolled, heat treated, pickled, and skin passed. The substrates were cleaned by sonication in acetone and ethanol. Then the substrates were rinsed with deionized water and dried.

The SiO_2 solution for the coating was made from tetraethyl orthosilicate ($C_8H_{20}O_4Si$ > 98%, VWR), isopropyl alcohol (C_3H_7OH > 99.5%, VWR), nitric acid (HNO_3, 65%, VWR), and deionized water. In the experiment, 5 ml tetraethyl orthosilicate and 8 ml isopropyl alcohol were mixed. After mixing them for 15 min, 2 ml water and 0.25 ml nitric acid were introduced, and the solution was stirred for 2 h. In the next step, 0.25 ml of SiO_2 solution was spin coated on the substrates at 1500 rpm for 20 s. The spin coated samples were first dried at room temperature for a few minutes and then in a furnace at 100 °C for 15 h.

The TiO_2 solution for the coating was made from tetra-*n*-butyl orthotitanate ($C_{16}H_{36}Ti$ > 98%, VWR), isopropyl alcohol (C_3H_7OH > 99.5%, VWR), ethyl acetoacetate ($C_6H_{10}O$ > 98%, VWR), nitric acid (HNO_3, 65%, VWR), and deionized water. In the experiments, 5 ml tetra-*n*-butyl orthotitanate, 40 ml isopropyl alcohol and 2 ml ethyl acetoacetate were mixed. After mixing for 15 min, 1 ml deionized water and 0.25 ml nitric acid were added and the solution was stirred for 2 h. 0.25 ml of the prepared TiO_2 solution was then spin coated at 1500 rpm for 20 s on three types of substrates: stainless steel plates, stainless steel plates which were previously coated with a layer of SiO_2 and stainless steel plates that were already coated with TiO_2. The coating step then yielded single-layer TiO_2 (SL-TiO_2), SiO_2/TiO_2 and double-layer TiO_2 (DL-TiO_2) samples, respectively. The coated plates were dried at room temperature for a few minutes and in a furnace at 100 °C for 15 h. Then, the plates were heat treated in the furnace at 400 °C for 2 h. For the double-layer TiO_2 samples, the coating and the heat treatment procedures were repeated, with a fresh TiO_2 solution (made by the method described above) being used for the coating step. It is emphasized that the two TiO_2 coatings (SL-TiO_2, DL-TiO_2) were prepared in order to find out the effect of the TiO_2 layer thickness on the photocatalytic activity of the sample.

2.2. Microstructural characterization

Surface and cross section of the synthesized coatings were studied using a field-emission scanning electron microscope (FE-SEM) Zeiss Ultraplus at an acceleration voltage of 15 kV. Cross-sectional studies were conducted in the plane-of-fracture of fractured samples tilted to approximately 22° with respect to the electron beam of FE-SEM. Compositional analyses of the coated surfaces were carried out using Inca 350 energy-dispersive spectrometer (EDS) attached to FE-SEM.

The crystal structure of the prepared coatings was determined with Raman spectroscopy and X-ray diffraction (XRD). Raman spectra were measured with an Andor Shamrock 303 spectrograph and a cooled CCD-camera Newton 940P. The excitation laser was a 532 nm wavelength Cobolt Samba with a beam diameter of 0.7 mm. The XRD measurements were carried out with a PANalytical Empyrean X-ray diffractometer and monocromatized CuKα radiation (λ = 1.5418 Å) with a scanning rate of 0.2° min^{-1} over a range of 20° < 2θ < 60° with low incident angle of radiation (1°). The data were analysed with HighScore plus software. The program employs The International Centre for Diffraction Data (ICDD) for phase analysis and Scherrer formula for crystal size measurement.

2.3. Determination of photocatalytic activity

Photocatalytic activities of the prepared samples were measured in the aqueous solution of methylene blue (MB, $C_{16}H_{18}ClN_3S$, VWR), which is also a widely used dye in the textile industry and also a model compound in many photocatalytic studies. The exact description of the photocatalytic degradation pathway of MB was published by Houas et al. (2001) [36]. The samples were placed into 30 ml of 0.015 mM MB solution in an open beaker and kept in the dark for 1 h in order to reach the adsorption equilibrium. After that, an ultra violet (UV) lamp Ledia NIS330U-M UV-Gun (wavelength maximum 365 ± 5 nm, light intensity 100 W/m^2), located above the MB solution, was turned on. During the photocatalytic reaction, the absorbance of MB in the solution was measured at 1 h time intervals by UV–vis spectroscopy (Shimazu UV-2501PC Spectrophotometer). A dark reference experiment was performed in otherwise identical conditions without UV irradiation. The discoloration of MB under UV irradiation but without the samples was also tested to exclude possible photolysis.

2.4. Photoelectrochemical measurements

Photoelectrochemical properties of the samples were characterized using potentiodynamic i–V scans, open circuit potential (OCP) monitoring and electrochemical impedance spectroscopy (EIS) measurements combined with the same UV lamp as was used for photoactivity determination. The measurements were carried out both under light intensity of 4 W/m^2 and without illumination.

The intensity was determined using a Photo/Radiometer HD2102.2 with a LP471 UVA probe (Delta Ohm Italy).

Photoelectrochemical measurements were carried out in a borate buffer solution containing 0.075 M $Na_2B_4O_7{\cdot}10H_2O$ and 0.05 M H_3BO_3 and featuring a pH value of 9.1; it is conductive enough for electrochemical measurements and harmless to the produced coatings. It is emphasized that methylene blue solution was not employed in electrochemical tests because it may take part in electrochemical reactions; borate buffer solution is inert in this respect.

The measurements were performed using a classical three-electrode cell (K0235 Flat Cell, Princeton Applied Research) with the sample of interest, i.e., SL-TiO_2, SiO_2/TiO_2, and DL-TiO_2, as a working electrode, a silver–silver chloride (Ag/AgCl, 3.0 M KCl) reference electrode and a platinum counter electrode as well as a Gamry Instruments potentiostat G750. Potentiodynamic scans were run from −1000 to 1200 mV vs. ref. at the rate of 5 mV s^{-1} in order to measure the generated current. OCP monitoring was performed for 3600 s (1 h). Electrochemical impedance measurements were conducted at the open circuit potential with 10 mV amplitude of perturbation in the frequency range from 5 mHz to 100 KHz. In each case, the measurements were performed for at least two replicate samples. The recorded EIS data was analyzed using a Gamry Echem Analyst 5.5 software by fitting resistive-capacitive electrical equivalent circuits to the data. The presented model employs constant phase elements (CPE) instead of capacitors; CPE equals to $1/C(j\omega)^n$, where n is the frequency dispersion factor and may obtain values in the range from 1 to 0 (when $n = 1$, C can be considered a real capacitance), j is the square root of −1 and ω is the angular frequency.

3. Results and discussion

3.1. Surface morphology

FE-SEM images of the SL-TiO_2, SiO_2/TiO_2, and DL-TiO_2 coatings and, in order to understand the electrochemical data, e.g., electron transfer processes, also of SiO_2 layer, are presented in Fig. 1a–d. All coatings were uniform and so thin that the surface features, such as the grain structure, of 2B stainless steel surface were clearly distinguished in the coating morphology. A closer examination, the results of which are shown in the insets, revealed that all coatings contained some cracks, typical of coatings produced by sol–gel technique. SL-TiO_2 had a slightly smoother morphology (Fig. 1a) as compared to the SiO_2/TiO_2 coating (Fig. 1b), evidently due to the presence of only one coating layer. Furthermore, the SiO_2/TiO_2 coating contained more cracks than TiO_2. The possible reason for the cracks detected in the SiO_2/TiO_2 coating is a greater overall thickness of the coating, resulting in easy cracking during the heat treatment at 400 °C. However, the DL-TiO_2 (Fig. 1c) clearly had fewer cracks than the coatings in SL-TiO_2 or SiO_2/TiO_2; the probable reason is the preparation procedure in which the drying and the heat treatment of the DL-TiO_2 sample were made layer by layer. It may also be readily noticed that SiO_2 coating (Fig. 1d) had a quite uniform surface although some cracks were evident in the structure. The relative thicknesses of the coating layers

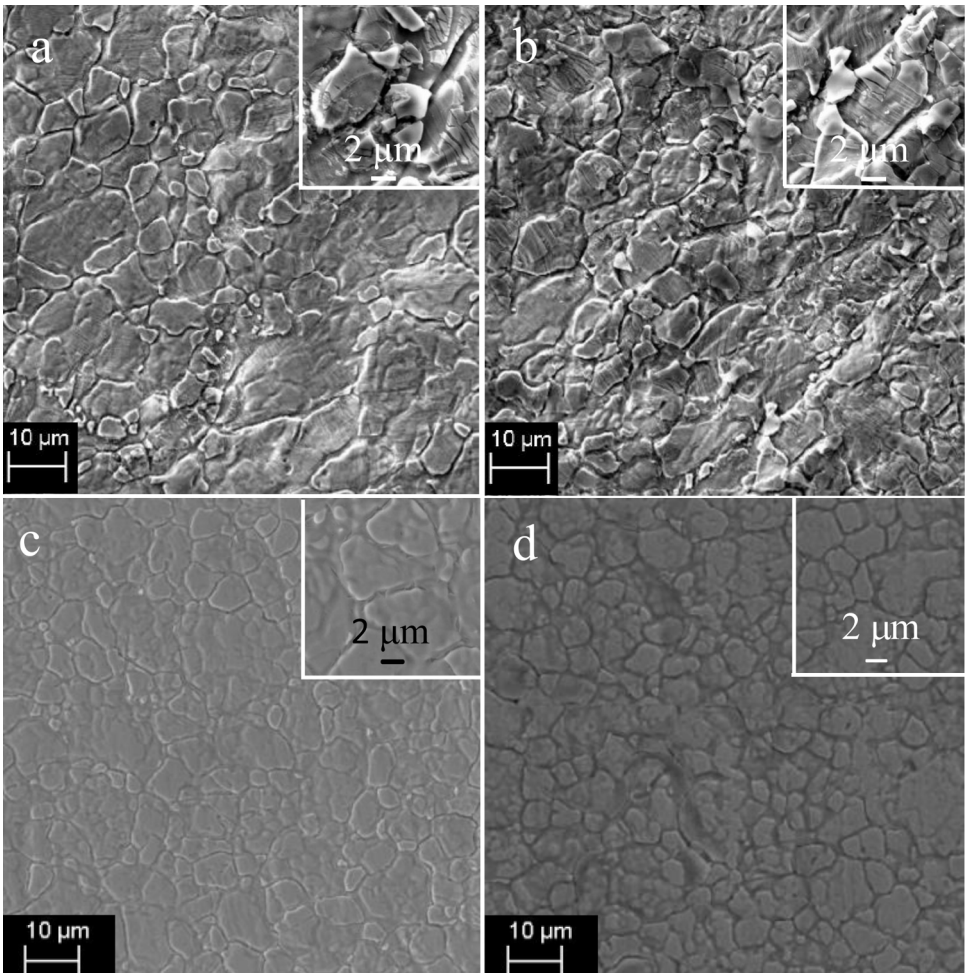

Fig. 1. FE-SEM micrographs of SL-TiO_2 (a), SiO_2/TiO_2 (b), DL-TiO_2 (c) and SiO_2 (d).

(SL-TiO_2, DL-TiO_2, SiO_2/TiO_2) may be deduced from the EDS analyses taken from the sample surfaces. According to the EDS analyses, the amount of Ti detected on the surfaces was 1.6, 4.8, and 5.0 wt.% for SL-TiO_2, DL-TiO_2, and SiO_2/TiO_2, respectively, indicating that the TiO_2 layer was essentially thinner in SL-TiO_2 than in DL-TiO_2 and SiO_2/TiO_2 samples. In turn, the amount of quantified Si was less than 1 wt.% for SL-TiO_2 and DL-TiO_2 samples and probably originated from the stainless steel substrate, but essentially more than 10 wt.% for SiO_2/TiO_2 and SiO_2 samples.

3.2. Cross-sectional examination

The plane-of-fracture micrographs of the SL-TiO_2, SiO_2/TiO_2, DL-TiO_2 and SiO_2 coating are presented in Fig. 2a–d and enable thickness of the coating layers to be determined. The overall thickness of the TiO_2 layer varied from 150 to 200 nm in SL-TiO_2 sample (Fig. 2a) and from 350 to 400 nm in SiO_2/TiO_2 sample (Fig. 2b). The examination of DL-TiO_2 sample revealed the total thickness of the TiO_2 layer to be in the range from 350 to 400 nm (Fig. 2c), like it was in the case of SiO_2/TiO_2 sample. In addition to the TiO_2 layer, the intermediate SiO_2 layer was detected between the TiO_2 layer and the substrate in the SiO_2/TiO_2 sample (Fig. 2b), with thickness varying in the range from 200 to 300 nm. This observation was confirmed by the plane-of-fracture micrograph taken from the SiO_2 coating (Fig. 2d). These observations are well consistent with the results from EDS analyses.

3.3. Crystal structure

3.3.1. Raman spectra

Analysis of the Raman spectra (Fig. 3) for the coatings confirmed that TiO_2 included in the samples was predominantly the anatase phase. The peaks observed in the spectra for all samples were approximately at 148 cm^{-1}, 402 cm^{-1}, 520 cm^{-1}, and 643 cm^{-1}, which agree very well with the reference values for anatase. The peaks for rutile would be located at 235 cm^{-1}, 445 cm^{-1}, and 605 cm^{-1} but are clearly absent from all three measured spectra [37]. In the case of SiO_2/TiO_2 sample, no peaks related to the SiO_2 layer at 430 cm^{-1}, 495 cm^{-1} and 606 cm^{-1} [38] were detected either, probably because it is retained beneath the TiO_2 layer.

3.3.2. XRD spectra

Fig. 4 shows the XRD spectra for the SL-TiO_2, SiO_2/TiO_2 and DL-TiO_2 coatings on a stainless steel substrate. Due to the overall thinness of the produced coatings, much of the XRD data originated from the substrate that contained austenite and ferrite phases. As for the synthesized coatings, neither anatase phase nor any other phase related to TiO_2 was detected by XRD technique in the SL-TiO_2 sample. This is probably due to the low thickness of the TiO_2 coating. It has been reported for a TiO_2 coated-soda lime glass that the XRD peaks of the anatase phase appear only when the coating thickness exceeds 500 nm [30]. However, in our study, a small peak (1 0 1) related to the anatase phase (ICDD 00-021-1272) was detected at 25.3° in 2θ scale in the XRD spectrum for SiO_2/TiO_2 and DL-TiO_2 samples even though the thickness of the TiO_2 coating was below 400 nm. The existence of (1 0 1) was clearly due to a relatively slow scanning rate and low incident angle of the radiation. Yet no peaks related to the SiO_2 layer were observed in the XRD spectrum for SiO_2/TiO_2 sample, probably because of the amorphous nature of SiO_2 synthesized at 400 °C. The crystallite size of TiO_2 anatase estimated by HighScore plus software was ~10 nm for both SiO_2/TiO_2 and DL-TiO_2 samples which is well consistent with previous studies in which the TiO_2 coating was prepared by sol–gel

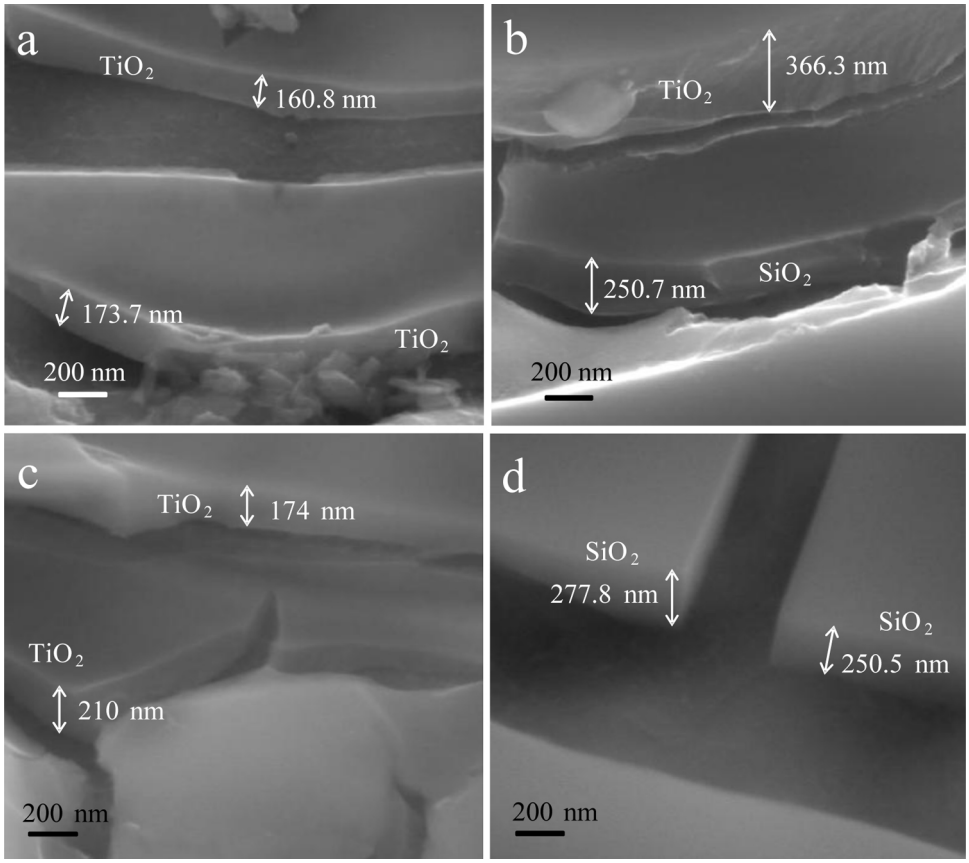

Fig. 2. The plane-of-fracture FE-SEM micrographs of SL-TiO_2 (a), SiO_2/TiO_2 (b), DL-TiO_2 (c) and SiO_2 (d). In Fig. 2b and c, the outer TiO_2 layer was cracked in a way that enabled also the examination of the inner layers.

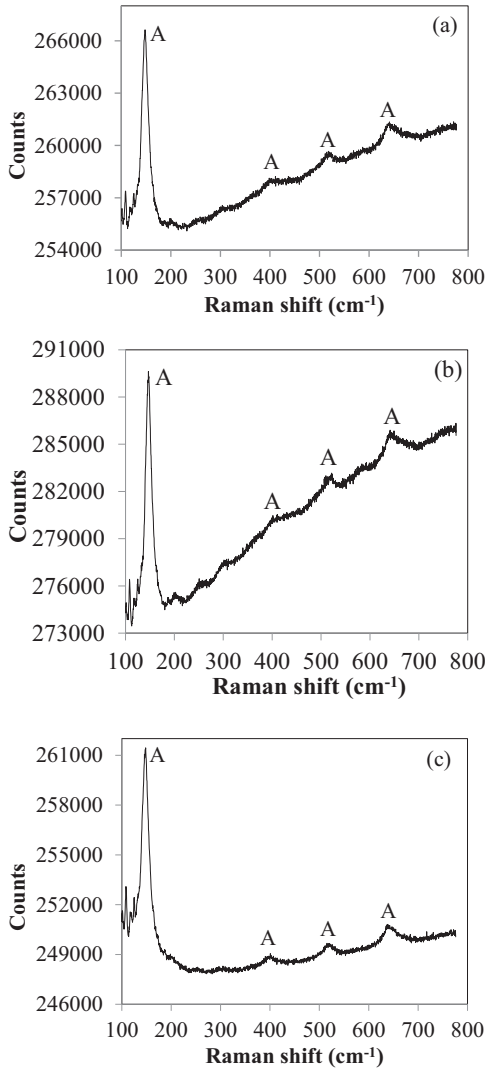

Fig. 3. Raman spectra for SL-TiO_2 (a), SiO_2/TiO_2 (b) and DL-TiO_2 (c).

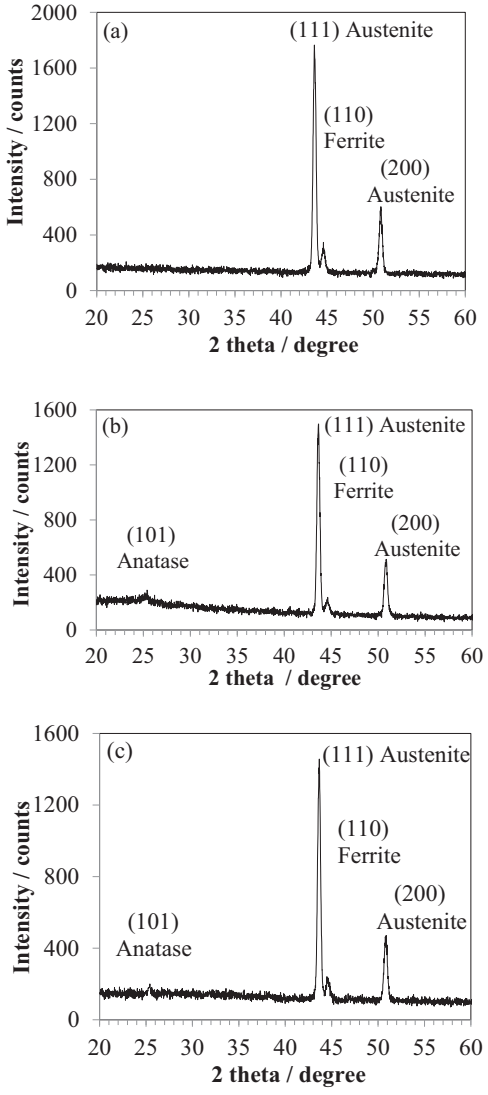

Fig. 4. XRD patterns for SL-TiO_2 (a), SiO_2/TiO_2 (b) and DL-TiO_2 (c).

method and heat treated at 400 °C [39,40]. Although the crystallite size of anatase was not possible to be estimated to SL-TiO_2 because of lack of the visible peaks of TiO_2, it can be supposed to be at the same level as those of SiO_2/TiO_2 and DL-TiO_2 because of the same heat treatment temperature (400 °C).

3.4. Photocatalytic efficiency of the coatings

The photocatalytic degradation of MB has been chosen as a model reaction to evaluate the photocatalytic activities of the synthesized coatings. The results of a relative absorbance of MB at the wavelength of 665 nm and as a function of irradiation time using SL-TiO_2, DL-TiO_2 and SiO_2/TiO_2 samples are shown in Fig. 5a–c. It can be seen that all prepared samples were photoactive. The dark experiment showed that there was no significant adsorption of MB on the prepared samples. It is also noteworthy that the irradiation of MB without the samples did not influence the concentration of MB, which means that the direct photolysis was excluded. As was expected on the basis of the literature, there was no practical difference in the photoactivity between SL-TiO_2 (Fig. 5a) and DL-TiO_2 (Fig. 5b) samples. Both exhibited a relatively slow degradation rate of MB, with only about 10% of MB being degraded after 6 h, even though the TiO_2 coating in the DL-TiO_2 sample was thicker than in the SL-TiO_2 sample. Indeed, according to the literature, the

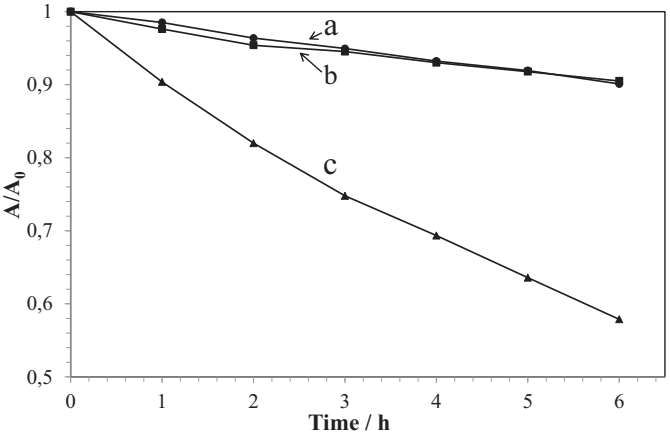

Fig. 5. Relative absorbance of MB at a wavelength 665 nm of SL-TiO_2 (a), DL-TiO_2 (b), and SiO_2/TiO_2 (c) as a function of irradiation time.

thickness of the TiO_2 coating drastically influences the photocatalytic activity of the coating only if the thickness is smaller than the depletion layer width, typically less than 100 nm [41]. However, there was a notable difference in the photocatalytic activity of SiO_2/TiO_2 sample as compared to the SL-TiO_2 and DL-TiO_2 samples (Fig. 5c). Indeed, the photocatalytic degradation yield for the SiO_2/TiO_2 sample was approximately 40% after 6 h.

Because the differences in the photocatalytic activity of the systems cannot be explained by the inherent thickness of the TiO_2 coatings nor the different crystal sizes, the explanation for the dissimilar performance needs to be found elsewhere. All in all, these results clearly demonstrate that the intermediate SiO_2 layer between the stainless steel substrate and the TiO_2 film had a significant beneficial influence on the photocatalytic activity of the SiO_2/TiO_2 sample.

It has been reported in literature that the light absorption of mixed TiO_2/SiO_2 powder particles was higher than that of corresponding pure TiO_2 [42]. However, such behavior was observed only in the wavelength range from 200 to 300 nm, which was not used in this study. Moreover, there is no evidence of the enhanced photocatalytic activity by the synergistic effect between the TiO_2 and SiO_2 phases [42]. Hence, the synergetic effect in which the separation of the charge carriers has been enhanced by connecting different materials or phases together [43] is not the probable explanation for a better photocatalytic activity of SiO_2/TiO_2 than TiO_2 samples in this work. Still, cotton samples coated with a mixture of TiO_2 and SiO_2 have shown a greater photocatalytic activity as compared with samples functionalized with pure TiO_2 [44]. The provided explanations were that SiO_2 increased, first, the specific surface area of the coating as compared to the use of pure TiO_2 and, second, the acidity of the surface, which may have raised the amount of hydroxyl groups on the surfaces and led to a greater amount of adsorbed water molecules. In this work, the SiO_2 layer is mostly underneath the TiO_2 layer, implying that the explanations given above do not hold here. Literature also reports on one case, where TiO_2 and SiO_2 are located on top/under one another. The photocatalytic activity of TiO_2 nanoparticles enclosed within a SiO_2 shell has been found to be significantly weaker than that of pure TiO_2. It has been stated that the photocatalytic activity of TiO_2 cores is suppressed by the SiO_2 coating because of the insulating properties of SiO_2 and the formation of poorly conductive Ti—O—Si bonds at the core–shell interface [45]. We emphasize that in our study, the intermediate SiO_2 layer in the SiO_2/TiO_2 sample was underneath the TiO_2 coating. Consequently, the SiO_2 layer acted as an insulator between the stainless steel substrate and the TiO_2 layer rather than between the TiO_2 layer and the surrounding environment. This enables us to conclude that the electrical properties of the system have to be considered.

3.5. Photoelectrochemical properties of the coatings

To obtain a deeper understanding on the photocatalytic and photoelectrochemical behavior of the produced coatings, it is necessary to consider the movement of charges, i.e., the transition of negatively charged electrons and positively charged holes, in a semiconductor material during excitation. It is well known that anatase TiO_2 is an *n*-type semiconductor. When such semiconducting material is illuminated with the photons of high energy, electron photoemission is possible. The more interesting case occurs when the photon energy is lower than the electron work function in the solution, i.e., the total work performed to transfer the electron into the solution, but still higher than the band gap of the semiconductor, i.e., the narrow energy gap, 3.2 eV, between the filled valence band and the empty conduction band situated energetically above. In such case, photoexcitation may introduce inter-band electron transitions from the valence band to the conduction band. Indeed, the result of such transition is the formation of a pair of free charge carriers, an electron in the conduction band and a positive hole in the valence band. Hence, the electrons and holes produced in pairs are separated in space.

It is known that only part of the photons absorbed by the TiO_2 may contribute to the generation of photocurrent due to, e.g., recombination and relaxation processes [46]. Therefore, i–V curves were determined for SL-TiO_2, SiO_2/TiO_2 and DL-TiO_2 samples under dark and illumination, Fig. 6. It may be noticed that, independently of the coating system under examination, the cur-

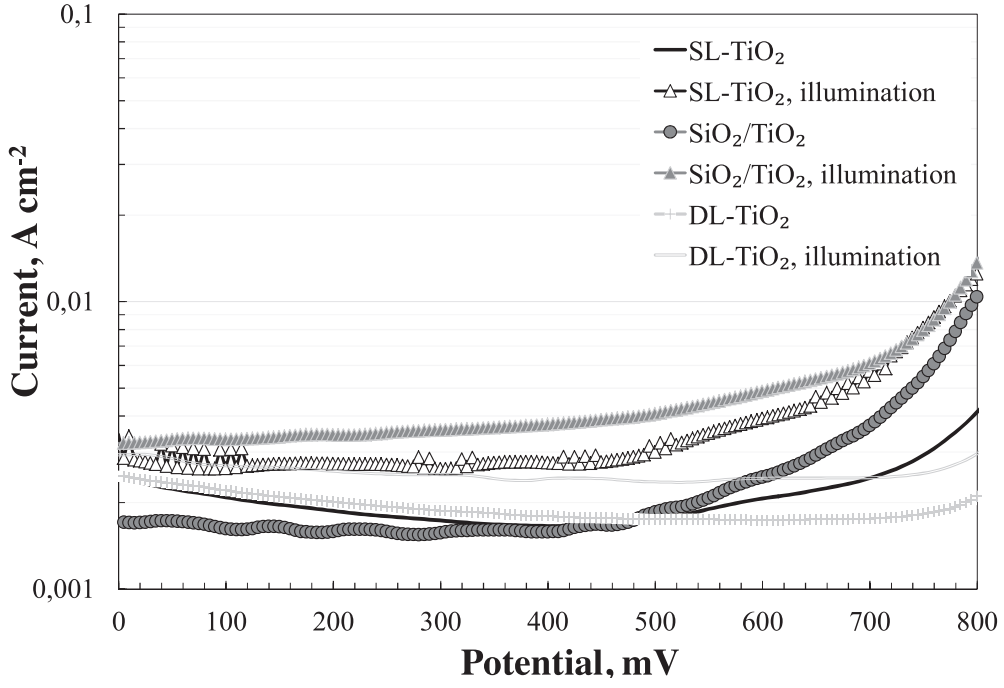

Fig. 6. i–V curves for the studied coating systems under non-illuminated and illuminated conditions.

rent values were systematically higher under illumination than in the absence of it, referring to photocurrent generation. All through the anodic potential range of interest (which was chosen to be well below the potential where oxygen evolution starts, about 1200 mV vs. Ag/AgCl), the obtained current values were highest for the SiO_2/TiO_2 sample under illumination and also the difference between the illuminated and non-illuminated conditions was greatest for the SiO_2/TiO_2 sample. This suggests that the use of intermediate SiO_2 layer may be used to improve the photo-conversion efficiency of TiO_2 coating-stainless steel system. This is consistent with the findings of Cao et al. [47], who used several ultrathin SiO_2 interlayers to improve the photo-conversion efficiency of hematite coating. Here, however, the generated photocurrent density, roughly 3.0 mA cm^{-2} at 0.6 V vs. Ag/AgCl, was even higher than that reported by Cao et al. [47] for their $[Fe_2O_3/SiO_2]_n/Fe_2O_3$ system, 1.13 mA cm^{-2} at 0.6 V vs. Ag/AgCl. It may also be seen that the use of thicker TiO_2 coating, DL-TiO_2, actually yields lower photocurrent than the use of a thinner TiO_2 coating, SL-TiO_2. It is further emphasized that i–V curves were also measured for the bare stainless steel substrate, but the results were essentially identical in dark and under illumination and the current levels much below those detected for the coating systems, indicating that the substrate does not contribute to photocurrent generation and implying that the detected photocurrent is essentially due to the applied coatings.

The results from open circuit potential monitoring are shown in Fig. 7. OCP values for the TiO_2 coating showed a steady increase from about −100 mV to approximately −20 mV vs. Ag/AgCl during the test period. When the same sample was illuminated, the OCP values were consistently somewhat lower, in the range from −240 to −200 mV vs. Ag/Ag all through the test. OCP measurements conducted for the sample containing a combination of silica and titania coatings, SiO_2/TiO_2, gave somewhat higher overall values than for the TiO_2 coating, increasing steadily from 0 mV to approximately 40 mV during the measurement. Under illumination, the OCP values for the SiO_2/TiO_2 coated sample were retained at a constant value of −280 mV vs. Ag/AgCl all through the test, thus being lower than for the TiO_2 sample. In the case of DL-TiO_2 sample, OCP values were clearly much lower than in other two coating systems under both non-illuminated and illuminated conditions. When illumination was not used, OCP values steadied at the level of about −240 mV vs. Ag/AgCl, while under illumination, the corresponding level was at about −320 mV vs. Ag/AgCl. The results from OCP monitoring enable two key trends to be observed. First, the values recorded for all three studied systems; TiO_2, SiO_2/TiO_2 and DL-TiO_2, under illumination were systematically shifted towards more

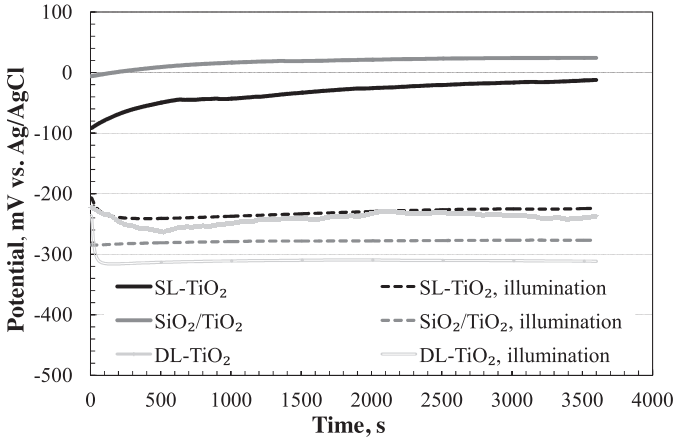

Fig. 7. OCP monitoring for TiO_2, SiO_2/TiO_2 and DL-TiO_2 samples without and under illumination.

negative values than without illumination. This is typical behavior of an *n*-type semiconductor [48]. Second, application of the silica film underneath the TiO_2 film (SiO_2/TiO_2 vs. TiO_2) shifted the OCP values for the non-illuminated sample towards positive potentials and those for the illuminated sample towards negative potentials, leading to a clearly greater difference in OCP values between the non-illuminated and illuminated states for SiO_2/TiO_2 than for TiO_2. This is an indication of a more effective generation of photoinduced charge carriers in the case of SiO_2/TiO_2 than of TiO_2. Evidently the smallest difference between the non-illuminated and illuminated states materialized for DL-TiO_2 sample, referring to an impaired generation of photoinduced charge carriers as compared to TiO_2 or SiO_2/TiO_2 samples.

In general, in *n*-type semiconductors, band gap edges are bent upwards, meaning that excess electrons in the conduction band will be driven from the surface into the semiconductor, while positive holes in the valence band will be pushed against the solution boundary. These matters together lead to stabilization of the excited state, creation of some steady concentration of excess electrons in the conduction band (inside the semiconductor) and excess holes in the valence band (at the semiconductor-solution interface). When the *n*-type semiconductor electrode is then illuminated (under open circuit conditions), the space charge in its surface layer will decrease under the effect of the holes accumulating at the surface, called an electron depletion region, and the electrode potential will move to the negative direction. This behavior has been explained in the literature by the means that positive holes on the surfaces can attract negatively charged species extracted from the solution to the surface of semiconductor [48]. Indeed, this is exactly what we observed for all our three coating systems: SL-TiO_2, SiO_2/TiO_2 and DL-TiO_2, in OCP measurements. Furthermore, the greater potential difference between the dark and illuminated states for SiO_2/TiO_2 than for TiO_2 (both SL and DL) suggests an essentially greater photoexcitation in the case of SiO_2/TiO_2 coating system, evidently due to enhanced charge carrier separation.

Electrochemical impedance spectra for the samples are presented in Fig. 8. The Nyquist plots for TiO_2 samples (both SL and DL) contained one semicircular arc, whereas those for the SiO_2/TiO_2 samples contained two semicircular arcs, suggesting one and two time constants for the systems, respectively (Fig. 8a and b). The Bode magnitude plot (Fig. 8c) at low frequencies revealed much higher total impedance values for the non-illuminated samples than for the illuminated counterparts, reflecting better electrical insulation properties of the non-illuminated samples. By implication, this may also be interpreted as the effective generation of photoinduced electrons and holes. The Bode phase angle plots (Fig. 8d) confirmed the observation about one and two time constant systems in the case of TiO_2 (both SL and DL) and SiO_2/TiO_2 samples, respectively, since as many maxima could be detected in the spectra. Each time constant, in turn, refers to a unique surface process. Because FE-SEM examination revealed that the coatings completely cover the stainless steel substrate, the probable explanation is that the surface processes arise from the different types of coating layers, i.e., TiO_2 and SiO_2 layers. Quantitative analysis of EIS spectra by fitting of the electrical equivalent circuits for one and two time constant systems (Fig. 9) enables us to explain the charge carrier generation phenomena in more detail. The numerical values obtained from data analysis are given in Table 1.

For comparison, we performed the corresponding EIS measurements for bare stainless steel (SS) substrates exposed to heat (oxidation) treatments at 400 °C for 2 h (SL-TiO_2) and 4 h (SiO_2/TiO_2 and DL-TiO_2), with the extracted values also being presented in Table 1. The fact that these substrate samples are characterized by two time constants is consistent with, e.g., findings on oxide films thermally grown at 600 °C on ferritic stainless steels [49], while the TiO_2 samples are described by one time constant only, supports the

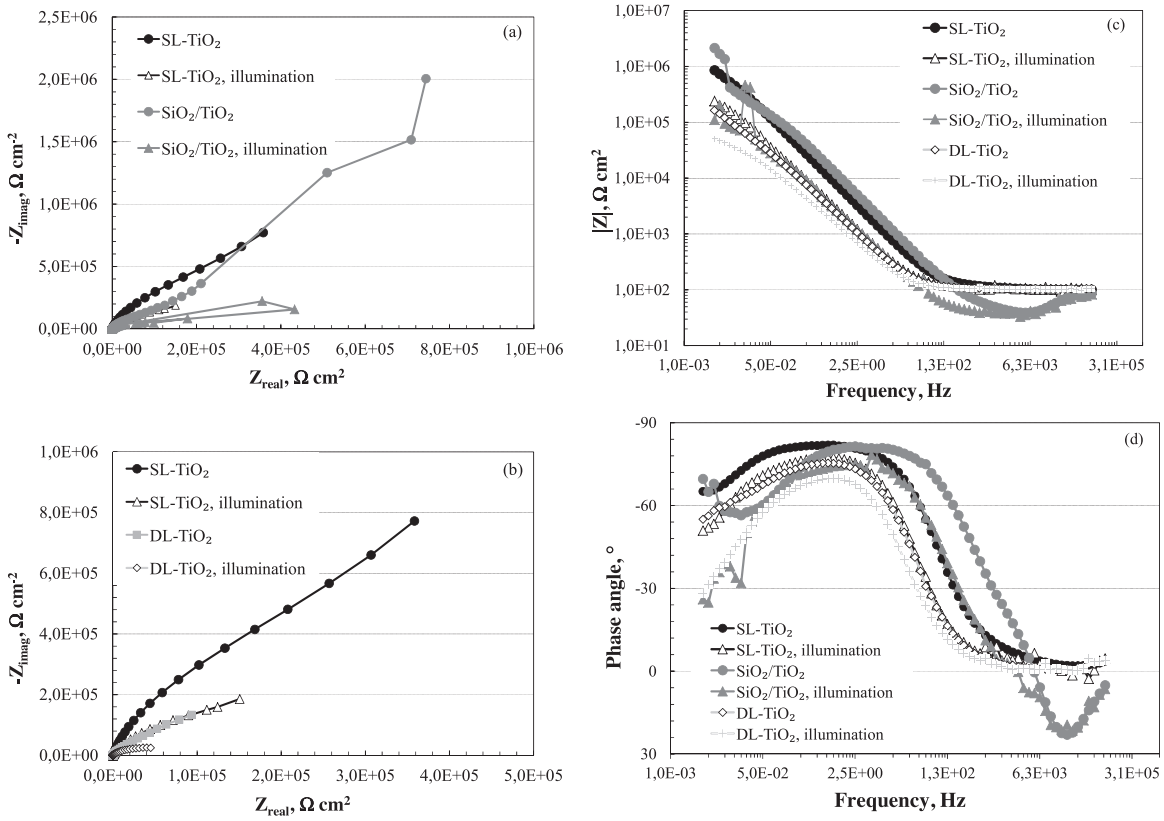

Fig. 8. EIS spectra for TiO_2, SiO_2/TiO_2 and DL-TiO_2 samples. (a and b) Nyquist plots. (c) Bode magnitude plots. (d) Bode phase angle plots.

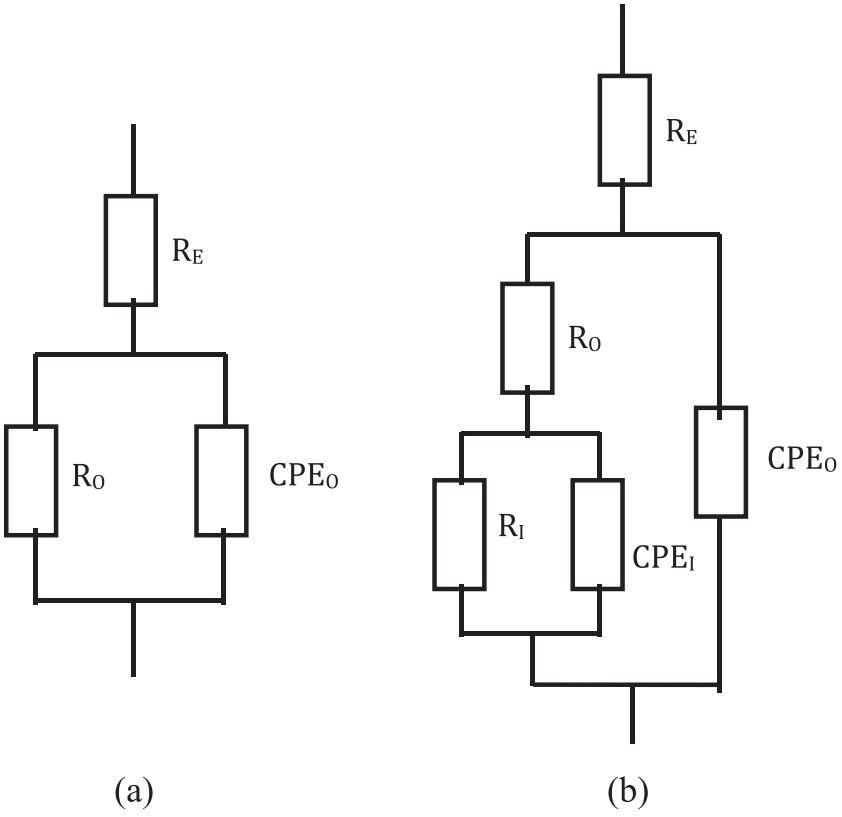

Fig. 9. Electrical equivalent circuits for the electrochemical systems. (a) One time constant model. (b) Two time constants model. R_E, R_O and R_I refer to the resistances of electrolyte, outer surface layer and inner surface layer, respectively. CPE is a constant phase element which is characterized by, e.g., a frequency dispersion factor *n*.

Table 1
Numerical values for electrical equivalent circuit components obtained from data analysis. *i* refers to illumination.

Sample	R_E, Ω cm^2	R_O, Ω cm^2	n	C_O, F cm^{-2}	R_I, Ω cm^2	n	C_I, F cm^{-2}	Model
TiO_2	103.9	2.3×10^6	0.90	1.3×10^{-5}				1 TC
TiO_2, *i*	104.4	4.0×10^5	0.88	1.2×10^{-4}				1 TC
SiO_2/TiO_2	45.7	7.5×10^5	0.90	2.8×10^{-5}	9.9×10^6	0.91	1.0×10^{-5}	2 TC
SiO_2/TiO_2, *i*	40.4	1.3×10^5	0.86	1.2×10^{-4}	3.6×10^5	0.82	1.1×10^{-2}	2 TC
DL-TiO_2	102.6	3.2×10^5	0.84	1.8×10^{-4}				1 TC
DL-TiO_2, *i*	101.7	5.9×10^4	0.82	2.7×10^{-4}				1 TC
SS, 2 h	114.1	8.8×10^5	0.93	2.0×10^{-5}	1.8×10^6	0.80	1.1×10^{-5}	2 TC
SS, 4 h	120.3	3.0×10^5	0.95	1.4×10^{-5}	9.6×10^6	0.99	9.7×10^{-6}	2 TC

In the case of stainless steel, the values are for bare substrate that has undergone heat (oxidation) treatment that corresponds to that included in the preparation of sol–gel coatings. Heat treatment was carried out at 400 °C for 2 h or 4 h. The measurements were done only without illumination because it is generally known that such thermally grown oxide films on stainless steel are not photoactive.
TC stands for time constant. Electrical equivalent model for 1 TC system is shown in Fig. 9a, while that for 2 TC system is shown in Fig. 9b.

view that the oxide films possibly developed on the substrate do not significantly contribute to the measured data. Furthermore, in the case of SiO_2/TiO_2 system, the values derived for the inner layer components, particularly for the capacitor, reflect that they are of different origin than the oxide films on the substrate.

As may be readily seen in Table 1, electrical resistance values were systematically lower under illumination than in dark, again demonstrating an improved charge carrier generation under illumination. We may also make some other important findings. First, in the case of SiO_2/TiO_2 system, the inner layer, i.e., the SiO_2 layer, systematically exhibits higher resistance values than the outer layer, i.e., the TiO_2 layer. Indeed, as high room-temperature electrical resistivity value as 1×10^{14} Ω cm has been reported for SiO_2 [50], supporting a view that the SiO_2 layer acts as a high-energy barrier for electron movement across it. Second, by comparing the values for outer layer resistance in DL-TiO_2 and SiO_2/TiO_2 samples that contain TiO_2 layer of a relatively equal thickness, it may be noticed that the resistance values are systematically somewhat higher in the case of SiO_2/TiO_2 system, referring essentially to a reduced electron movement in the TiO_2 layer in SiO_2/TiO_2 as compared to that in DL-TiO_2 coating. Third, the capacitance values for the SiO_2/TiO_2 system, especially for the SiO_2 layer, increase more radically than for the TiO_2 coating systems with shift from dark to illumination. Capacitance is related to the quantity of charge stored because of dielectric properties of the materials, i.e., separation of positively and negatively charged entities on a molecular or atomic level [51]. Capacitance is proportional to the dielectric constant for the material [51]. For SiO_2, dielectric constant values of 3.8 [52] and 4.42–4.6 [53] have been reported. The values reported for TiO_2 slightly vary between the references. In Ref. [53], dielectric constant values ranging from 33 to 54 have been obtained for the rutile phase. Groner and George [54] acknowledge that TiO_2 is characterized by dielectric constant values ranging from 50 to 110 and, within that range, rutile phase exhibits higher values than anatase phase. Furthermore, according to Kim et al. the dielectric constants are 41.3 and 145.2 for the pure anatase and rutile thin films, respectively [55]. Nevertheless, although the exact value is correlated to the references quoted and may also slightly depend on the used manufacturing method, it is evident that dielectric constant for anatase TiO_2 is much higher than that for SiO_2. The values under illumination have not been reported, but it is expected that in such cases, the values for titania would be even higher than in the dark. Therefore, the differences in materials dielectric behavior between anatase TiO_2 and SiO_2 cannot explain the observation about a much greater relative increase in capacitance value for SiO_2 than for TiO_2 layer with the use of illumination. We explain the observations as follows. It is clear that because of a high energy barrier posed by the SiO_2 layer, the produced photoelectrons cannot across the SiO_2 layer. Therefore, the photo-generated electrons become trapped in the SiO_2 layer and, with respect to electrochemistry, the SiO_2 layer acts as a dielectric under photocurrent and thereby improves the photoelectrochemical properties of the system, i.e., SiO_2 layer insulates the TiO_2 layer electrically from the substrate and consequently prevents continuous charge transfer to the substrate. This suggestion about the capacitive behavior of the SiO_2 layer is in agreement with the findings of Zhang et al. [56] and Sun et al. [57] yet both of these groups incorporated SiO_2 in the composite coating.

So far, the development of TiO_2 coatings with improved photoactive and photoelectrochemical properties has primarily concentrated on the methods to synthesize the TiO_2 coating, [27,34,58] the optimization of the following heat treatments [32] or the doping of the coatings [56,59,60]. However, as mentioned above, also the selection of the substrate material plays a key role with respect to the properties of the coating. What remains unconsidered in terms of systematic research effort is the role of the substrate in the charge transfer processes that are, nevertheless, the key issue in photoactivity. To our knowledge, there are only three attempts to improve the coating performance by playing with the electron transfer processes of the substrate [35,47,61]. First, comparison was done between the photoelectrochemical properties of TiO_2 coating applied on Ti substrate and Ti substrate oxidized at 500 °C [35]. It was found that the thermally grown oxide film beneath the photoactive coating improved the photoelectrochemical properties of the system due to the passivating nature of the thermal oxide film, which can suppress the back electron transfer from Ti substrate to the electrolyte [35]. Second, [61] similar TiO_2 films were deposited on stainless steel, indium tin oxide (ITO)-sputtered stainless steel and ITO- and SiO_x-sputtered stainless steel, with the ITO film being conductive but the SiO_x film essentially insulating, and the photoelectrochemical properties of the three coating systems were compared. The system with the SiO_x film yielded the best photoconversion efficiency, which was explained by the SiO_x film preventing the movement of charge carriers from stainless steel to the electrolyte. Cao et al. [47] attributed the improved photoelectrochemical properties of alternating Fe_2O_3 and SiO_2 layers on ITO glass as compared to plain Fe_2O_3 film to improved electron–hole migration inside the coating, and they specified the role of SiO_2 by the "generation of two depletion zones with opposite electric field direction". We think that this refers to the same phenomenon we observed, i.e., SiO_2 layers acting as a capacitor because of high-energy barrier by the SiO_2 layer probably insulates TiO_2 coating from the substrate.

Indeed, the results of this study confirmed that the application of the intermediate SiO_2 film hinders the unwanted moving of charge carriers from the TiO_2 coating to the stainless steel substrate. Besides, by the use of EIS method we could clearly demonstrate the important role the SiO_2 plays in the improved photocatalytic and photoelectrochemical properties: it acts as capacitor under illumination. This explains why the electrical conductivity by electron motion of the SiO_2 layer increased with a shift from dark to illumi-

Table 2
Results derived from EIS data.

Sample	f, Hz	τ, s	τ_d, s
SL-TiO_2	0.79	0.20	48
TiO_2–SiO_2	2.51	0.06	TiO_2: 15.6 SiO_2: 3960
DL-TiO_2	1.00	0.16	15.9

nation, indicating that the electrons in the conduction band of TiO_2 are driven towards the inner SiO_2 layer under illumination. Due to this, it is possible that some of the electrons finally penetrate the capacitive SiO_2 layer and reach the substrate. However, these are probably much fewer than in the absence of the SiO_2 layer. This is because the SiO_2 layer inhibits the movement of photoinduced electrons by a high-energy Schottky barrier between TiO_2 and the SiO_2 layers [48] and acting as a dielectric, causing most of the electrons to be trapped in the coating. Theoretically, the presence of the SiO_2 film could also inhibit the recombination of electrons and holes, an effect called passivation [62], which leads to a longer lifetime of the photoexcited state. However, the values for the effective charge lifetime (Table 2), derived from EIS data according to:

$$\tau = \frac{1}{2\pi f} \quad (1)$$

where τ is the lifetime of the charge (electron) and f is the characteristic frequency, corresponding to the peak in Bode phase angle plot in the intermediate-frequency regime [35,63], do not support such idea. Another parameter worth evaluation is the electron transfer time, τ_d, within each layer. τ_d may be defined as [64]:

$$\tau_d = R \times C \quad (2)$$

where R and C and resistance and capacitance values from fitting. The values for the electron transfer time in each case are shown in Table 2.

Clearly, the order of electron transport time τ_d of different layers is consistent with our view that electrons are retained within the SiO_2 film and that the increased electron movement within the SiO_2 layer to be due to some of the electrons entering the SiO_2 layer and being stored there (capacitor). Also the presence of cracks in the SiO_2 layer and, probably, TiO_2 coating filling such areas, may contribute to the enhanced electron movement. Indeed, one direction for the future studies will be the optimization of the microstructure of both TiO_2 and SiO_2 layers with respect to the photoelectrochemical performance. After the coating microstructure optimization is done, the photoelectrochemical measurements will be conducted in electrolyte that correspond to real application environments more closely (although care has to be taken not to damage the coatings chemically).

4. Conclusion

In this study, we have prepared TiO_2 coatings on the stainless steel substrate without and with an intermediate layer of SiO_2. Both TiO_2 and SiO_2 coatings were synthesized using a sol–gel method. The prepared coating systems were characterized in terms of microstructure, photocatalytic activity and photoelectrochemical properties. The following conclusions may be drawn on the basis of the presented results:

1) The photocatalytic efficiency of TiO_2 coating on the stainless steel substrate can be significantly enhanced by the application of an intermediate layer of SiO_2.
2) The photocatalytic efficiency of anatase TiO_2 is not a direct function of the TiO_2 coating thickness. We observed that the photocatalytic efficiencies for TiO_2 films of two thicknesses were roughly the same.
3) EIS measurements revealed that the intermediate layer of SiO_2 features high electrical resistance and insulates TiO_2 coating from substrate. Under illumination, SiO_2 layer acts as a dielectric (capacitor) with a lowered electrical resistance as compared to situation in dark. Because of the capacitive behavior of the SiO_2 inner layer, the electrons lifetime within the SiO_2 layer is very long, enabling less electrons to move to the substrate. Such behavior of the SiO_2 layer contributes to a greater photocurrent values detected for SiO_2/TiO_2 system than for TiO_2 coating.
4) The fact that the SiO_2 layer acts as a capacitor is related to the fact that the SiO_2 layer poses a high-energy barrier for electron movement. Consequently, electrons are insulated from the substrate.
5) EIS measurements provide an excellent tool for determining the role of each coating layer in the photocatalytic and photoelectrochemical properties.

Acknowledgement

The present study is supported by Finnish Graduate School on Advanced Materials and Processes.

References

[1] W. Wang, M. Ding, C. Lu, Y. Ni, Z. Xu, Appl. Catal. B: Environ. 144 (2014) 379–385.
[2] M. Nischk, P. Mazierski, M. Gazda, A. Zaleska, Appl. Catal. B: Environ. 144 (2014) 674–685.
[3] J. Reszczynska, T. Grzyb, J.W. Sobczak, W. Lisowski, M. Gazda, B. Ohtani, A. Zeleska, Appl. Catal. B: Environ. 163 (2015) 40–49.
[4] H. Lachheb, E. Puzenat, A. Houas, M. Ksibi, E. Elaloui, C. Guillard, J.-M. Herrmann, Appl. Catal. B: Environ. 39 (2002) 75–90.
[5] S. Danwittayakul, M. Jaisai, J. Dutta, Appl. Catal. B: Environ. 163 (2015) 1–8.
[6] A. Turki, C. Guillard, F. Dappozze, Z. Ksibi, G. Berhault, H. Kochkar, Appl. Catal. B: Environ. 163 (2015) 404–414.
[7] K. Hashimoto, H. Irie, A. Fujishima, TiO_2 photocatalysis: a historical overview and future prospects, AAPPS Bull. 17 (2007) 12–28.
[8] A. Maury Ramirez, K. Demeestere, N. De Belie, T. Mäntylä, E. Levänen, Build. Environ. 45 (2010) 832–838.
[9] A. Fujishima, K. Hashimoto, T. Watanabe, Photocatalysis Fundamentals and Applications, BKC, Tokyo, 1999.
[10] M.K. Nazeeruddin, A. Kay, I. Rodicio, R. Humbhry-Baaker, E. Mueller, P. Liska, N. Vlachopoulos, M. Grätzel, J. Am. Chem. Soc. 115 (1993) 6382–6390.
[11] A. Hagfeld, M. Grätzel, Chem. Rev. 95 (1995) 49–68.
[12] I. Exnar, L. Kavan, S.Y. Huang, M. Grätzel, J. Power Sources 68 (1997) 720–722.
[13] T. Watanabe, A. Nakajima, R. Wang, M. Minabe, S. Koizumi, A. Fujishima, K. Hashimoto, Thin Solid Films 351 (1999) 260–263.
[14] A. Fujishima, T.N. Rao, D.A. Tryk, J. Photochem. Photobiol. C: Photochem. Rev. 1 (2000) 1–21.
[15] D.A.H. Hanaor, C.C. Sorrell, J. Mater. Sci. 46 (2011) 855–874.
[16] S. Yin, H. Hasegawa, D. Maeda, M. Ishitsuka, T. Sato, J. Photochem. Photobiol. A: Chem. 163 (2004) 1–8.
[17] P. Zhang, S. Yin, T. Sato, Mater. Res. Bull. 45 (2010) 275–278.
[18] G. Li, L. Chen, M.E. Graham, K.A. Gray, J. Mol. Catal. A: Chem. 275 (2007) 30–35.
[19] D.C. Hurum, A.G. Agrios, K.A. Gray, J. Phys. Chem. B 107 (2003) 4545–4549.
[20] J.-P. Nikkanen, T. Kanerva, T. Mäntylä, J. Cryst. Growth 304 (2007) 179–183.
[21] J.-P. Nikkanen, E. Huttunen-Saarivirta, T. Kanerva, V. Pore, T. Kivelä, E. Levänen, T. Mäntylä, J. Ceram. Sci. Technol. 2 (2011) 97–102.
[22] J.-P. Nikkanen, E. Huttunen-Saarivirta, X. Zhang, S. Heinonen, T. Kanerva, E. Levänen, T. Mäntylä, Ceram. Int. 40 (2014) 4429–4435.
[23] S. Yin, R. Li, Q. He, T. Sato, Mater. Chem. Phys. 75 (2002) 76–80.
[24] P. Zhang, S. Yin, T. Sato, Mater. Res. Bull. 45 (2010) 275–278.
[25] J.-P. Nikkanen, S. Heinonen, E. Huttunen Saarivirta, M. Honkanen, E. Levänen, IOP Conf. Ser.: Mater. Sci. Eng. 47 (2013) 012066.
[26] M. Aromaa, H. Keskinen, J.M. Mäkelä, Biomol. Eng. 24 (2007) 543–548.
[27] M. Aromaa, A. Arffman, H. Suhonen, J. Haapanen, J. Keskinen, M. Honkanen, J.-P. Nikkanen, E. Levänen, M.E. Messing, K. Deppert, H. Teisala, M. Tuominen, J. Kuusipalo, M. Stepien, J.J. Saarinen, M. Toivakka, J.M. Mäkelä, J. Aerosol Sci. 52 (2012) 57–68.
[28] J.-P. Nikkanen, M. Harju, M. Järn, J. Linden, J. Rintala, M.E. Messing, E. Huttunen-Saarivirta, T. Saarinen, T. Kanerva, M. Honkanen, M. Aromaa, E. Levänen, M. Pettersson, J.M. Mäkelä, K. Deppert, T. Mäntylä, Powder Technol. 266 (2014) 106–112.
[29] J. Harra, J.-P. Nikkanen, M. Aromaa, H. Suhonen, M. Honkanen, T. Salminen, S. Heinonen, E. Levänen, J.M. Mäkelä, Powder Technol. 243 (2013) 46–52.
[30] J. Yu, X. Zhao, Mater. Res. Bull. 35 (2000) 1293–1301.

[31] U.L. Stangar, U. Cernigoj, P. Trebse, K. Maver, S. Gross, Monatsh. Chem. 137 (2006) 647–655.
[32] A. Fernandez, G. Lassaletta, V.M. Jimenez, A. Justo, A.R. Gonzalez-Elipe, J.-M. Herrmann, H. Tahiri, Y. Ait-Ichou, Appl. Catal. B: Environ. 7 (1995) 49–63.
[33] R. Mechiakh, R. Bensaha, C.R. Phys. 7 (2006) 464–470.
[34] A. Maury-Ramirez, J.-P. Nikkanen, M. Honkanen, K. Demeestere, E. Levänen, N. De Belie, Mater. Charact. 87 (2013) 74–85.
[35] K. Fan, T. Pen, B. Chai, J. Chen, K. Dai, Electrochim. Acta 55 (2010) 5239–5244.
[36] A. Houas, H. Lachheb, M. Ksibi, E. Elaloui, C. Guillard, J.-M. Herrmann, Appl. Catal. B: Environ. 31 (2001) 145–157.
[37] W. Ma, Z. Lu, M. Zhang, Appl. Phys. A 66 (1998) 621–627.
[38] A. Rahmani, M. Benoit, C. Benoit, Phys. Rev. B 68 (2003) 1–11, 184202.
[39] D.J. Kim, S.H. Wang, S.H. Oh, E.J. Kim, Mater. Lett. 57 (2002) 355–360.
[40] N. Barati, M.A. Faghihi Sani, H. Ghasemi, Z. Sadeghian, S.M.M. Mirhoseini, Appl. Surf. Sci. 255 (2009) 8328–8333.
[41] C.-Y. Wu, Y.-L. Lee, Y.-S. Lo, C.-J. Lin, C.-H. Wu, Appl. Surf. Sci. 280 (2013) 737–744.
[42] J. Aguado, R. Van Grieken, M.-J. Lopez-Munoz, Z. Marugan, Appl. Catal. A: Gen. 312 (2006) 202–212.
[43] D.O. Scanlon, C.W. Dunnill, J. Buckeridge, S.A. Shevlin, A.J. Logsdail, S.M. Woodley, C. Richard, A. Catlow, M.J. Powell, R.G. Palgrave, I.P. Parkin, G.W. Watson, T.W. Keal, P. Sherwood, A. Walsh, A.A. Sokol, Nat. Mater. 12 (2013) 798–801.
[44] E. Pakdel, W.A. Daoud, J. Colloid Interface Sci. 401 (2013) 1–7.
[45] H.S. Lee, S.M. Koo, J.W. Woo, J. Ceram. Process. Res. 13 (2012) 300–303.
[46] R. Li, Q. Li, L. Zong, X. Wang, J. Yang, Electrochim. Acta 91 (2013) 30–35.
[47] J. Cao, L. Liu, A. Hashimoto, J. Ye, Electrochem. Commun. 48 (2014) 17–20.
[48] V.S. Bagotsky, Fundamentals of Electrochemistry, John Wiley & Sons, New Jersey, 2006.
[49] E. Huttunen-Saarivirta, V.-T. Kuokkala, P. Pohjanne, Corros. Sci. 87 (2014) 344–365.
[50] W.Z. Zhu, S.C. Deevi, Mater. Sci. Eng. A 348 (2003) 227–243.
[51] B.R. Hinderliter, D.G. Croll, D.E. Tallman, Q. Su, G.P. Bierwagen, Electrochim. Acta 51 (2006) 4505–4515.
[52] H. Treichel, B. Withers, G. Ruhl, P. Ansmann, R. Würl, Ch. Müller, M. Dietlmeier, G. Maier, Low dielectric constant materials for interlayer dielectrics, in: H.S. Nalwa (Ed.), Handbook of Low and High Dielectric Constant Materials and Their Applications, Materials and Processing, vol. 1, Academic Press, San Diego, USA, 1999.
[53] W.M. Haynes, CRC Handbook of Chemistry and Physics, 95th ed., Taylor&Francis Group, Boca Raton, USA, 2014–2015.
[54] M.D. Groner, S.M. George, High k-dielectrics grown by atomic layer deposition: capacitor and gate applications, in: S.P. Murarka, M. Eizenberg, A.K. Sinha (Eds.), Interlayer Dielectrics for Semiconductor Technologies, Academic Press, San Diego, 2003.
[55] J.Y. Kim, H.S. Jung, J.H. No, J.-R. Kim, K.S. Hong, J. Electroceram. 16 (2006) 447–451.
[56] J.J. Zhang, J.-M. Hu, J.-Q. Zhang, C.-N. Cao, Int. J. Hydrogen Energy 36 (2011) 5218–5226.
[57] M. Sun, X. Zhang, J. Li, X. Cui, D. Sun, Y. Lin, Electrochem. Commun. 16 (2012) 26–29.
[58] F.-L. Toma, D. Sokolov, G. Bertrand, D. Klein, C. Coddet, C. Meunier, J. Therm. Spray Technol. 4 (2006) 576–581.
[59] W. Mekprasart, T. Khumtong, J. Rattanarak, W. Techitdheera, W. Pecharapa, Energy Procedia 34 (2013) 746–750.
[60] V. Pore, M. Heikkilä, M. Ritala, M. Leskelä, S. Areva, J. Photochem. Photobiol. A: Chem. 177 (2006) 68–75.
[61] M.G. Kang, N.G. Park, K.S. Ryu, S.H. Chang, K.-J. Kim, Sol. Energy Mater. Sol. Cells 90 (2006) 574–581.
[62] S. Smit, D. Garcia-Alonso, S. Bordhin, M.S. Hanssen, W.M.M. Kessels, Sol. Energy Mater. Sol. Cells 120 (2014) 376–382.
[63] R. Kern, R. Sastrawan, J. Ferber, R. Stangl, J. Luther, Electrochim. Acta 47 (2002) 4213–4225.
[64] K. Fan, T. Peng, J. Chen, K. Dai, J. Power Sources 196 (2011) 2939–2944.